ENGINEERING APPLICATIONS OF COMPUTATIONAL FLUID MECHANICS
2021, VOL. 15, NO. 1, 512–529
https://doi.org/10.1080/19942060.2021.1893820

Effects of in-line deflectors on the overall performance of a channel heat exchanger

Younes Menni [a], Houari Ameur[b], Mohsen Sharifpur[c,d] and Mohammad Hossein Ahmadi [e]

[a]Unit of Research on Materials and Renewable Energies (URMER), Abou Bakr Belkaid University of Tlemcen, Tlemcen, Algeria; [b]Department of Technology, University Centre of Naama – Ahmed Salhi, Naama, Algeria; [c]Institute of Research and Development, Duy Tan University, Da Nang, Viet Nam; [d]Department of Mechanical and Aeronautical Engineering, University of Pretoria, Pretoria, South Africa; [e]Faculty of Mechanical Engineering, Shahrood University of Technology, Shahrood, Iran

ABSTRACT
The turbulent convective thermal transfer in channel heat exchangers (CHEs) is studied numerically via the CFD (Computational Fluid Dynamics) method. Deflectors are inserted on the hot bottom walls of the heat channel to enhance the hydrothermal characteristics. Various shapes of in-line deflectors are considered, namely: rectangular ($a/b = 0.00$), cascaded rectangular-triangular ($a/b = 0.25$, 0.50, and 0.75), and triangular ($a/b = 1.00$) shapes. From the obtained results, the inclusion of in-line deflectors with $a/b = 0.75$ has given the most significant thermal enhancement factor, which was higher than that for $a/b = 0.00$, 0.25, 0.50, and 1.00 by about 5.36, 5.06, 67.27, and 3.88%, respectively. Also, the in-line cascaded deflector' case ($a/b = 0.75$) shows an increase in the enhancement factor (η) from 4 to 15.44% over the cases of one deflector (corrugated, rectangular, triangular, trapezoidal, arc, (+), S, 45° V, 45° W, T, Γ, and ε-shaped) or two deflectors (staggered corrugated). This highlights the effectiveness of in-line cascaded rectangular-triangular deflectors with $a/b = 0.75$ in improving the performance of the proposed exchanger for the conditions adopted.

ARTICLE HISTORY
Received 14 June 2020
Accepted 17 February 2021

KEYWORDS
Thermal transfer; forced convection; computational fluid dynamics; channel heat exchanger; deflectors

Introduction

The continuous increase of the global energy demand caused awareness about climate change and energy shortages. The renewable and environmentally sustainable energies, such as solar energy, have become an efficient alternative in various sectors, i.e. industrial, domestic, rural, etc.

The investigation of the performances of solar heat-exchangers (SHEs) is of extremely needed, since these devices are utilized in various industrial areas and vital applications. The enhancement of their efficiency remains still of great concern for engineers and users. One of the most effective ways for an important heat exchange (HE) within a smooth airway, such as cooling or heating solar ducts, with lower high flow rates, is the use of attached (Kadari et al., 2018) or detached (Kaewkohkiat et al., 2017), transverse (Hosseinirad et al., 2019) or longitudinal (Wang et al., 2019), orthogonal (Karmakar & Mohanty, 2019) or inclined (Phila et al., 2020), solid (Li et al., 2020a), slotted (Alfellag et al., 2020), perforated (Liu et al., 2019) or porous (Davari & Maerefat, 2016), and simple (Hanna et al., 2002), corrugated (Gholami et al., 2019) or shaped (Menni et al., 2020a) type inserts, known as vortex generators (VGs), turbulators, turbulence promoters, or deflectors (Awais & Bhuiyan, 2018; Huang et al., 2018), such as ribs, baffles, or fins (Ameur, 2019; Boukhadia et al., 2018), placed in parallel, in-line, or staggered arrays (Lee et al., 2018). These vortex generators are utilized to lengthen the trajectory of the fluid particles and to increase the interaction between them, which generates improved thermal efficiency.

Pipes and channels with attached and detached baffles, fins and ribs are the focus of many research works. Among them, Demartini et al. (2004) examined the details of the turbulent airflow in a duct equipped with two baffles. For a baffled duct heat exchanger, Ary et al. (2012) reported that two baffles yield greater thermal exchange rates than a single baffle and the number of holes has a considerable influence on the flow behavior. The study performed by Khan et al. (2002) revealed that the baffles create larger flow disturbance than that of the ribs. Promvonge and Thianpong (2008) carried out experiments to determine the hydrothermal characteristics of air through an exchanger provided with different shaped ribs (wedge, triangular, and rectangular) in in-line and staggered arrays. Hwang et al. (1999)

CONTACT Mohsen Sharifpur mohsensharifpur@duytan.edu.vn; mohsen.sharifpur@up.ac.za; Mohammad Hossein Ahmadi mohammadhosein.ahmadi@gmail.com

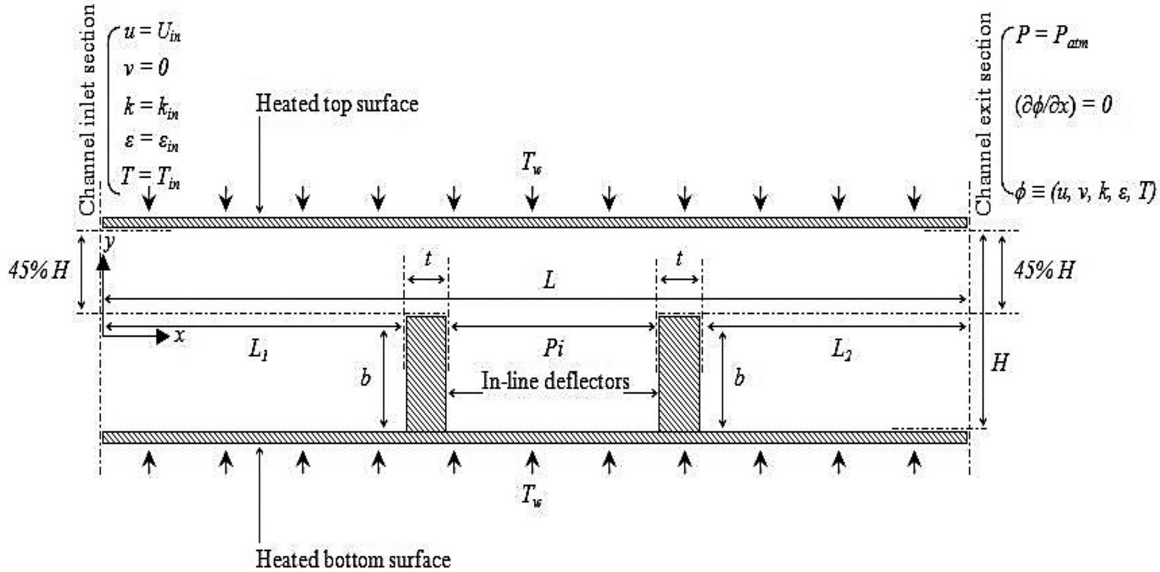

Figure 1. Computational domain of the problem studied.

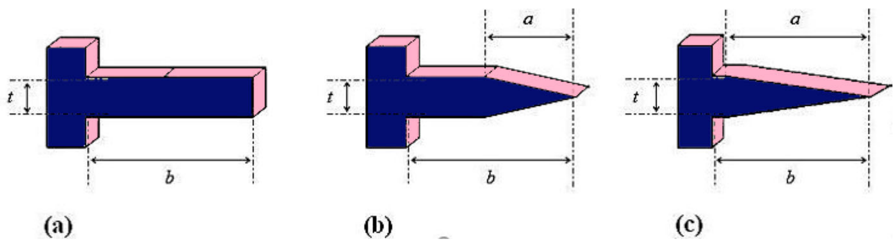

Figure 2. Geometrical configurations under analysis: (a) $a/b = 0.00$, (b) $a/b = 0.25$–0.75, and (c) $a/b = 1.00$.

predicted the effect of rib length on the turbulent flow characteristics inside a duct. Zhao et al. (2016) carried out experiments on the influence of pin density and shapes (triangle, circular, elliptical, and square) on the flow in a rectangular duct. Wang et al. (2012) inspected the flow and thermal exchange through a duct having various staggered pin fins, (drop, circular, and elliptical). Liu and Wang (2011) found in their study a significant enhancement in the local thermal exchange when using semi-attached ribs in channels. Ameur (2020) presented an investigation of the hydrothermal characteristics of a channel equipped with wavy baffles. Other researchers were interested in the investigation of the effect of baffle

Table 1. Structural parameters of the physical domain under study (Demartini et al., 2004).

Parameter [m]	Value
Length of the exchanger, L	0.554
Height of the exchanger, H	0.146
Width of the exchanger, W	0.193
Hydraulic diameter, D_h	0.167
Deflector thickness, t	0.010
Deflector height, b	0.080
Spacing, Pi	0.142
Inlet-1st deflector length, L_1	0.218
2nd deflector-exit length, L_2	0.174

Table 2. Thermal physical properties of air (ANSYS Fluent 12.0, 2012).

Parameter	Value
Density, $\rho_f (kg/m^3)$	1.225
Heat capacity, $Cp_f (J/kg.K)$	1006.43
Thermal conductivity, $\lambda_f (W/m.s)$	0.0242
Kinematic viscosity, $\mu_f (kg/m.s)$	1.7894×10^{-5}

Table 3. Necessary equations (Menni et al., 2020b; Yang & Hwang, 2003).

Equations	ϕ	Γ_ϕ	S_ϕ
Continuity	1	0	0
x-momentum	u	μ_e	$-\dfrac{\partial P}{\partial x}$
y-momentum	v	μ_e	$-\dfrac{\partial P}{\partial y}$
Energy	T	$\dfrac{\mu_e}{\sigma_T}$	0
Turbulent energy	k	$\mu_l + \dfrac{\mu_t}{\sigma_k}$	$-\rho\varepsilon + \mu_t\left\{2\left(\dfrac{\partial u}{\partial x}\right)^2 + 2\left(\dfrac{\partial v}{\partial y}\right)^2 + \left(\dfrac{\partial v}{\partial x} + \dfrac{\partial u}{\partial y}\right)^2\right\}$
Turbulent dissipation	ε	$\mu_l + \dfrac{\mu_t}{\sigma_\varepsilon}$	$\dfrac{\varepsilon}{k}(c_1 G - c_2 \rho\varepsilon)$

Table 4. Necessary parameters.

Prandtl number, $Pr(=0.71)$	$Pr = \frac{Cp_f \mu_f}{\lambda_f}$
Turbulent Prandtl number, $Pr_t(=0.85$ at the wall)	$Pr_t = \frac{\varepsilon_M}{\varepsilon_H}$
Reynolds number, *Re*	$Re = \frac{\rho_f U_{in} D_h}{\mu_f}$
Hydro-dynamic diameter of the exchanger, *Dh*	$D_h = \frac{2HW}{(H+W)}$
Friction factor, *f*	$f = \frac{(\Delta P/L) D_h}{\frac{1}{2}\rho_f U_{in}^2}$
Local coefficient of heat transfer, *h(x)*	$h(x) = \lambda_f \frac{T_w - T_p(x)}{y_p} \cdot \frac{1}{T_w - T_b(x)}$
Bulk temperature *Tb (x)*	$T_b(x) = \frac{\int_A u(x,y).T(x,y)dA}{\int_A u(x,y).dA}$
Local number of Nusselt, *Nux*	$Nu_x = \frac{h(x) D_h}{\lambda_f}$
Average number of Nusselt, *Nu*	$Nu = \frac{1}{L}\int Nu_x \partial x$
Hydrothermal performance, η (Menni et al., 2018a)	$\eta = \frac{(Nu/Nu_0)}{(f/f_0)^{1/3}}$
Nu0(for $Re \geq 10{,}000$) (Dittus & Boelter, 1930)	$Nu_0 = 0.023 Re^{0.8} \mathrm{Pr}^{0.4}$
f_0 (for $3{,}000 \leq Re \leq 5\times10^6$) (Petukhov, 1970)	$f_0 = (0.79 \ln Re - 1.64)^{-2}$

where, ε_M is the diffusivity for momentum transfer, ε_H is the diffusivity for heat transfer, ΔP is the pressure drop, *p* subscript is the 1st inner-node from the solid-wall, T_p is the temperature at the cell adjacent to the wall, y_p is the distance from point p to the wall, and Nu_0 and f_0 are the Nusselt number and friction factor for the smooth exchanger.

Table 5. Mesh density tests for $Re = 3.2 \times 104$ at ($0 \leq x \leq L$, $y = H/2$).

	Mesh nodes							
nx	95	120	145	170	195	220	**245**	370
ny	35	45	55	65	75	85	**95**	145
			***a/b* = 0.00**					
η	1.118	1.135	1.146	1.155	1.173	1.194	**1.201**	1.210
Er (%)	7.603	6.198	5.289	4.545	3.057	1.322	**0.784**	Ref.
			***a/b* = 0.25**					
η	1.129	1.139	1.164	1.170	1.180	1.199	**1.205**	1.216
Er (%)	7.154	6.332	4.276	3.782	2.960	1.398	**0.904**	Ref.
			***a/b* = 0.50**					
η	0.394	0.399	0.402	0.404	0.406	0.409	**0.415**	0.418
Er (%)	5.741	4.545	3.827	3.349	2.870	2.153	**0.717**	Ref.
			***a/b* = 0.75**					
η	1.181	1.201	1.225	1.231	1.241	1.255	**1.269**	1.283
Er (%)	7.950	6.391	4.520	4.053	3.273	2.182	**1.091**	Ref.
			***a/b* = 1.00**					
η	1.137	1.159	1.181	1.186	1.194	1.208	**1.220**	1.237
Er (%)	8.084	6.305	4.527	4.122	3.476	2.344	**1.374**	Ref.

inclination on the flow and thermal exchange behaviors (Eiamsa-ard and Chuwattanakul, 2020).Yongsiri et al. (2014) reported that, at high Reynolds number, the 60° and 120° inclination angles of ribs generate comparable thermal exchange rates and heat performance factors that are the most significant than those of the other cases. Promvonge et al. (2015) determined the influence of inclined horseshoes baffles on the overall efficiency of a tubular heat exchanger. For a duct fitted with inclined perforated vortex generators (VGs), Dutta and Hossain (2005) reported that the local thermal exchange is dependent on the design, orientation, and location of the 2ndVG. For an air heater channel, Bopche and Tandale (2009) determined the impact of U-shaped VGs inserted on the absorber surface. The U- and V-shaped baffles have also been studied by many researchers (Misra et al., 2020; Promvonge & Skullong, 2020). The porous baffles were also the subject of some investigations (Ameur & Menni, 2019; Mesgarpour et al., 2018). Detailed reviews on the various techniques to enhance the performance of CHEs (Channel heat-exchangers) may be found in the literature (Alam & Kim, 2017; Kabeel et al., 2017).

According to both the numerical and experimental models, it is well evident that finning technology has a sensitive effect on reinforcing the flow field and improving the heat transfer within CHEs. Several authors and engineers have studied and investigated different CHEs with very complex deflectors in an overlapping arrangement in most of their studies. In our proposed research, new models of in-line regular-deflectors are highlighted to increase the efficiency of CHEs. In the present analysis, steady-state, Newtonian, and incompressible flows of air over in-line deflectors in channels with in-line rectangular ($a/b = 0.00$), cascaded rectangular-triangular ($a/b = 0.25, 0.50$, and 0.75), and triangular ($a/b = 1.00$) shaped deflectors fitted to the hot bottom walls of CHEs are simulated and analyzed numerically. These deflectors direct the fluid flow to circulate in a very small section in the channel duct, to lengthen the trajectory of the fluid, to enhance the heat exchange surface, to force the recirculation zones, to create the turbulence and therefore a successful heat transfer. On the other hand, a comparison of the obtained optimum deflector performance with other deflectors from the literature (Menni et al., 2018a, 2018b) is shown to highlight the importance of the finning technique for such exchangers.

Mathematical modelling

Channel heat exchanger under study

The hydrothermal characteristics of a CHE are determined in this paper. The computational domain of the problem studied is given in Figure 1. It is a channel fitted with in-line transverse, vertical, and solid deflectors on its bottom wall. The channel length-to-hydraulic diameter, width-to-height aspect ratio of channel, deflector height-to-channel height, and deflector spacing-to-channel height ratio are fixed at, $L/D_h = 3.317$, $W/H = 1.321$, $h/H = 0.547$, and $Pi/H = 0.972$, respectively. These values were considered basing on the experiments of Demartini et al. (2004).

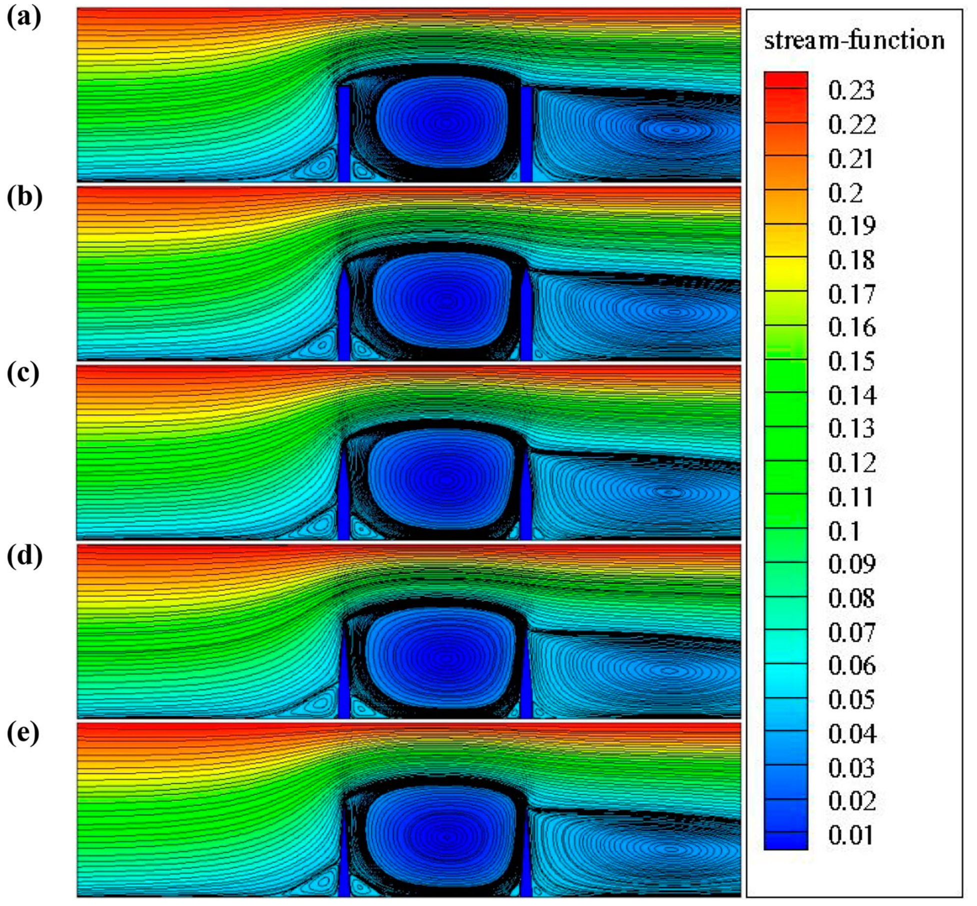

Figure 3. Mesh type for (a) $a/b = 0.00$, (b) $a/b = 0.25$, (c) $a/b = 0.50$, (d) $a/b = 0.75$, and (e) $a/b = 1.00$.

Vortex generators under investigation

Effects of the deflector shape were examined by realizing three geometrical cases, namely: flat rectangular ($a/b = 0$ or case A in Figure 2a), cascaded rectangular-triangular ($a/b = 0.25$, 0.50, and 0.75 or case B in Figure 2b), and triangular ($a/b = 1.00$ or case C in Figure 2c).

Used geometrical dimensions and materials' thermal-physical properties

The required details on geometrical parameters are summarized in Table 1. The thermal-physical properties of the working fluid (air) are summarized in Table 2.

Assumptions and hydrothermal boundary conditions

The study concerns turbulent flow and forced-convection of an incompressible Newtonian fluid ($Pr = 0.71$) with constant thermal physical properties and flowing inside a channel. The 2D steady-state with neglected radiation thermal exchange mode are treated. Air enters the exchanger at 300 K with zero pressure ($P_{in} = 0$) (Nasiruddin & Siddiqui, 2007). A uniform 1D velocity profile ($u = U_{\rm in}$, $v = 0$) is set at the exchanger inlet (Demartini et al., 2004). A temperature of 375 K is set on the entire walls of the exchanger (Nasiruddin & Siddiqui, 2007). The walls of the exchanger, as well as the deflectors, are considered impermeable and no-slip (Demartini et al., 2004). At the exchanger outlet, the atmospheric pressure is set $P_{ex} = P_{\rm atm}$ (Demartini et al., 2004). Further details on the theoretical and mathematical tools are provided in (Menni et al., 2020b; Yang & Hwang, 2003).

Governing equations and parameters

For these considerations, the governing-equations are given in the common form as follows(Menni et al., 2020c, 2021; Yang & Hwang, 2003):

$$\frac{\partial}{\partial x}(\rho u \varphi) + \frac{\partial}{\partial y}(\rho v \varphi) = \frac{\partial}{\partial x}\left[\Gamma_\varphi \frac{\partial \varphi}{\partial x}\right] + \frac{\partial}{\partial y}\left[\Gamma_\varphi \frac{\partial \varphi}{\partial y}\right] + S_\varphi \qquad (1)$$

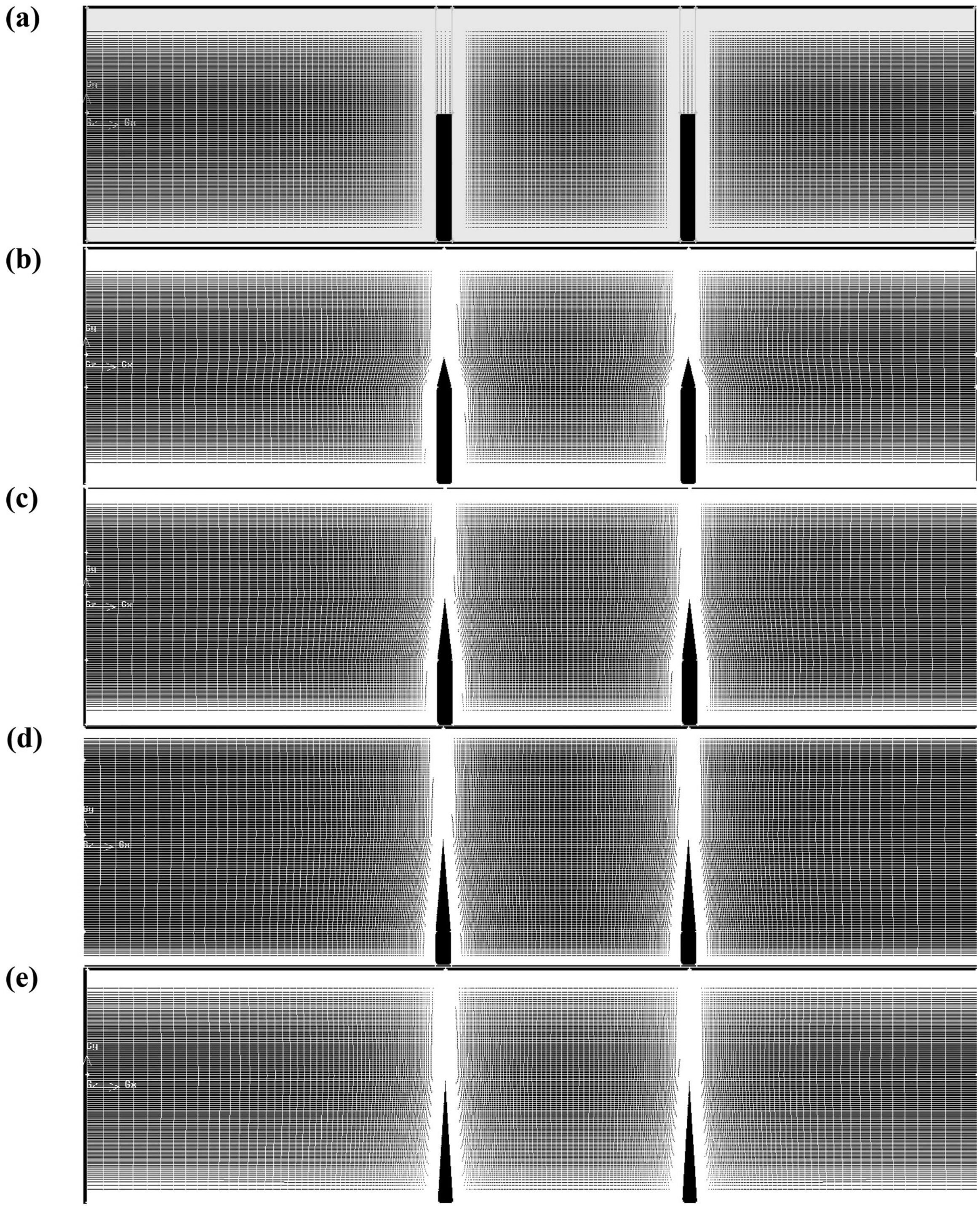

Figure 4. Verification of (a) Nu_0 and (b) f_0 for various turbulence models and Re numbers, using SIMPLE algorithm and Quick scheme.

where ϕ is a vector composed of the scalars u, v, T, k, and ε. Γ_ϕ is the turbulent diffusion coefficient, and S_ϕ is the ϕ source term associated (Table 3). The turbulent-air characteristics are modeled by the standard-type k-ε model (Launder & Spalding, 1974). All the parameters characterizing fluid transport and heat transfer are detailed in the following table (Table 4).

Numerical modelling

Numerical schemes

The Quick(Quadratic Upstream Interpolation for Convective Kinetics) scheme (Leonard & Mokhtari, 1990) and the SIMPLE(Semi Implicit Method for Pressure Linked Equations algorithm) algorithm (Patankar, 1980)

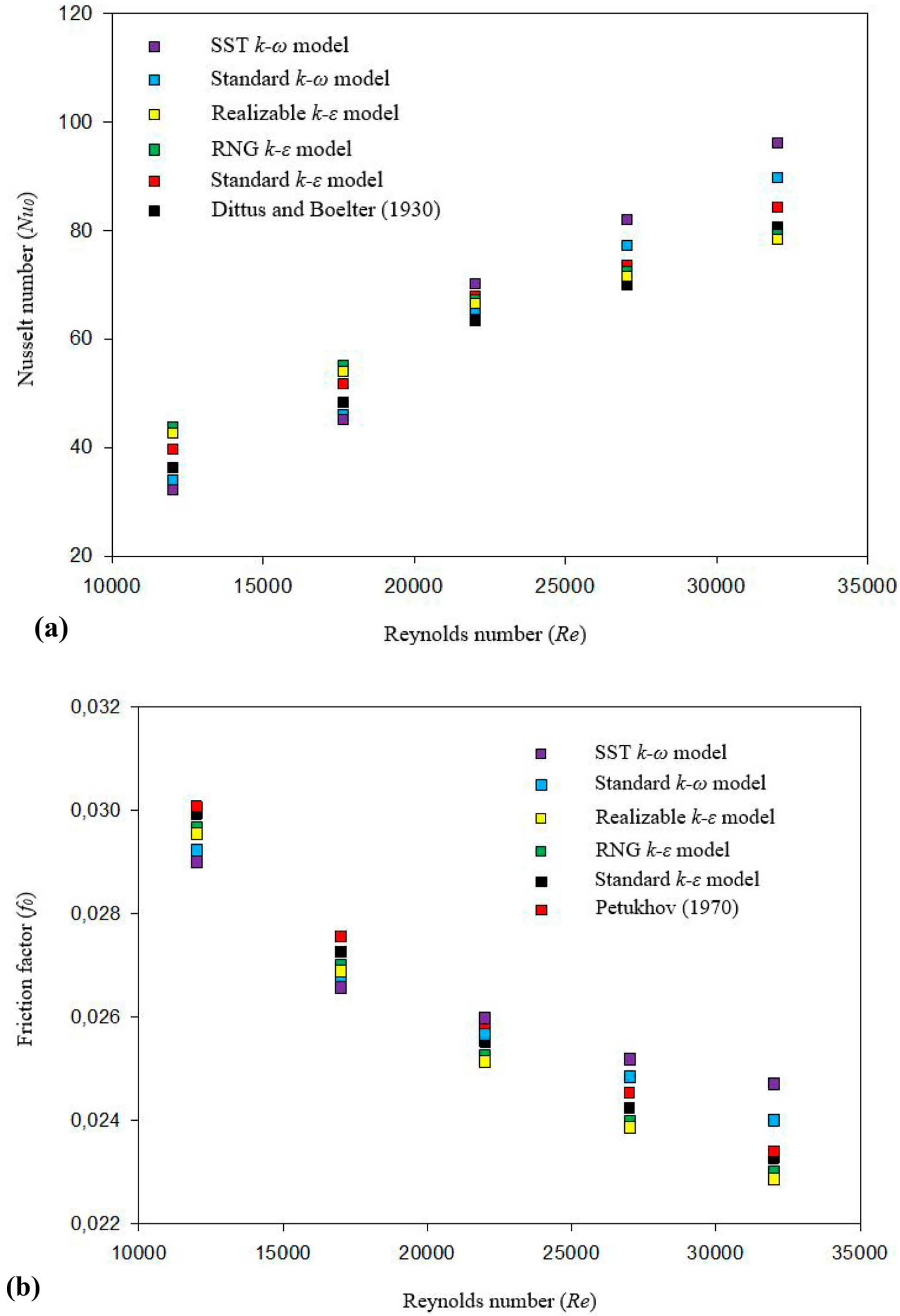

Figure 5. Streamlines at $Re = 12{,}000$, for (a) $a/b = 0.00$, (b) $a/b = 0.25$, (c) $a/b = 0.50$, (d) $a/b = 0.75$, and (e) $a/b = 1.00$.

were employed to achieve computations with the computer software 'ANSYS Fluent 12.0 (2012)'. The probed exchanger is simulated with a two-dimensional, non-uniform, structured, and quadrilateral mesh (Figure 3), as it is very concentrated near the solid boundary.

Mesh density tests

Several grids have been adopted with different $(n_x \times n_y)$ nodes, starting from 95 to 370 according to the horizontal axis, while from 35 to 145 according to the vertical axis. The performance values (η) were checked according to the hot top wall ($0 \le x \le L$, $y = H/2$) for

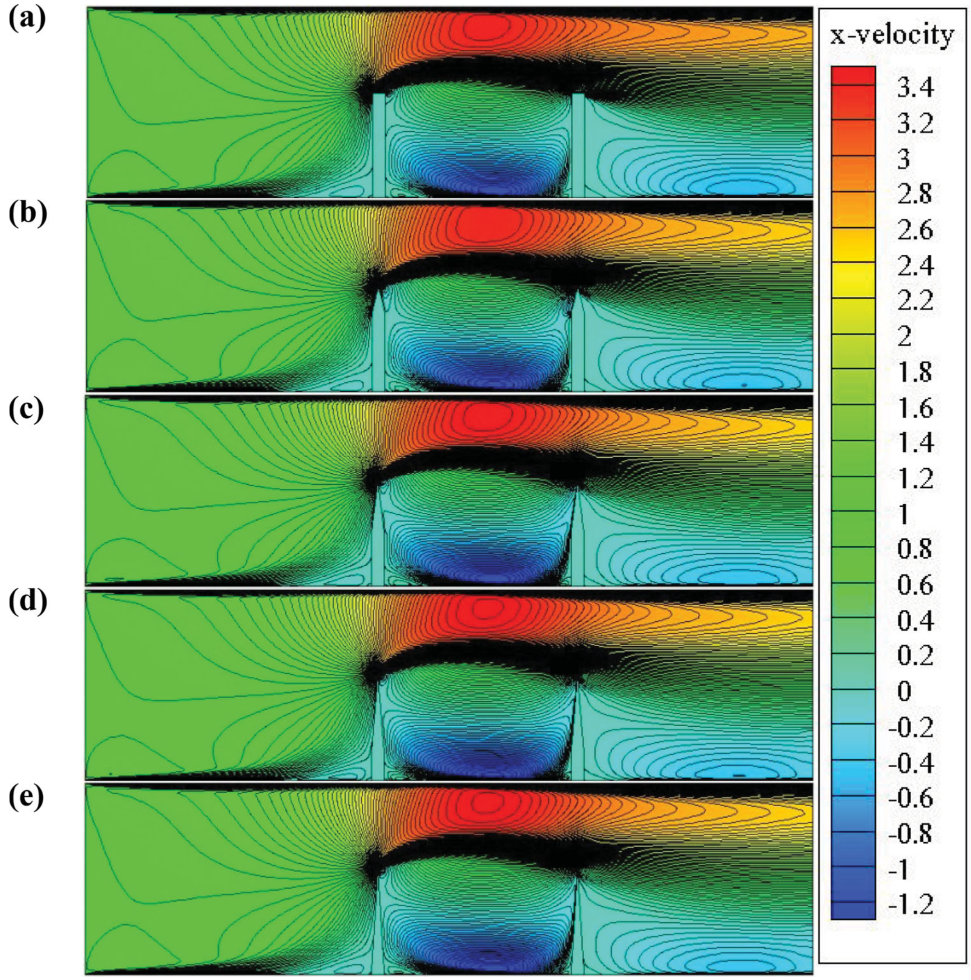

Figure 6. Axial velocity fields at $Re = 12{,}000$, for (a) $a/b = 0.00$, (b) $a/b = 0.25$, (c) $a/b = 0.50$,(d) $a/b = 0.75$, and (e) $a/b = 1.00$.

$Re = 3.2 \times 10^4$ and for all deflector models considered (Table 5). Comparing the different-cell results shows that it is not necessary to raise the number of cells from (245×95) to (370×145) since the relative error does not exceed 1 percent in the case of $a/b = 0.00$, 0.25 and 0.50 models, while it does not exceed 1.5 percent in the case of the remaining models ($a/b = 0.75$ and 1.00). Then, the incoming mesh of (245×95) nodes is built for all investigated models.

Turbulence model tests

Five different models are considered, namely (i) Standard -type k-ε, (ii) RNG-k-ε, (iii) Realizable-k-ε, (iv) Standard-type k-ω, and (v) SST-k-ω model. Beginning by the determination of the Nusselt number (Nu_0), where Nu_0 values are provided in Figure 4(a) in the case of $1.2 \times 10^4 \le Re \le 3.2 \times 10^4$. The results obtained by the five various two-equation models are verified against those calculated by the empirical correlation of Dittus and Boelter (1930). We note that these values are given for a smooth exchanger. Firstly, an increase in Nu_0 is noted with the rise of Re for all turbulence cases. The comparison plots between the different models revealed that the standard-k-ε type is able to provide satisfactory Nu_0 values over the range of Reynolds number used here. The standard-k-ω and SST-k-ω models gave excellent predictions at low Re, but the deviation from those of the correlation increased at high Re. However, it seems that the RNG-k-ε and realizable-k-ε model cases perform better at high Re (as observed for $Re \ge 2.2 \times 10^4$).

In the same smooth exchanger, the variation in the f_0 vs. Re is plotted in Figure 4(b) for the five types of two-equation models. Verification and comparison of these plots is made against the experimental data of Petukhov (1970). From this figure, it seems that the standard k-ε model remains the most efficient for all values of Re. However, a significant deviation is observed for the other models, where the realizable-k-ε case gave the lowest amounts of f_0 and the SST-k-ω yielded the greatest values of f_0 at high Re, especially at $Re = 3.2 \times 10^4$.

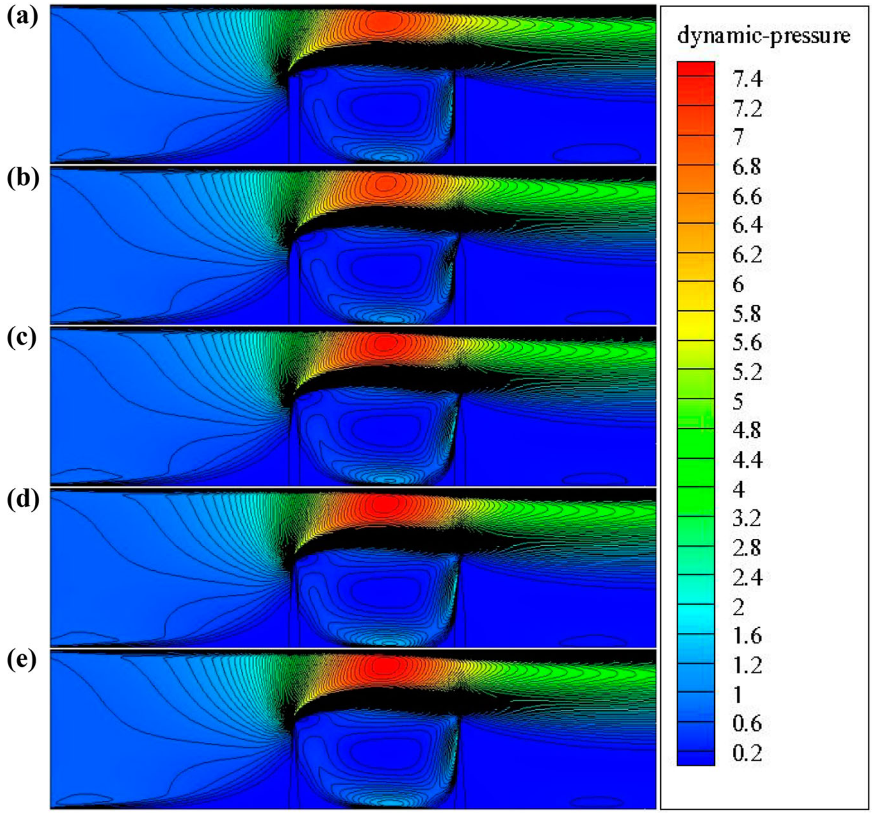

Figure 7. Distribution fields of the dynamic pressure at $Re = 12{,}000$, for (a) $a/b = 0.00$, (b) $a/b = 0.25$, (c) $a/b = 0.50$, (d) $a/b = 0.75$, and (e) $a/b = 1.00$.

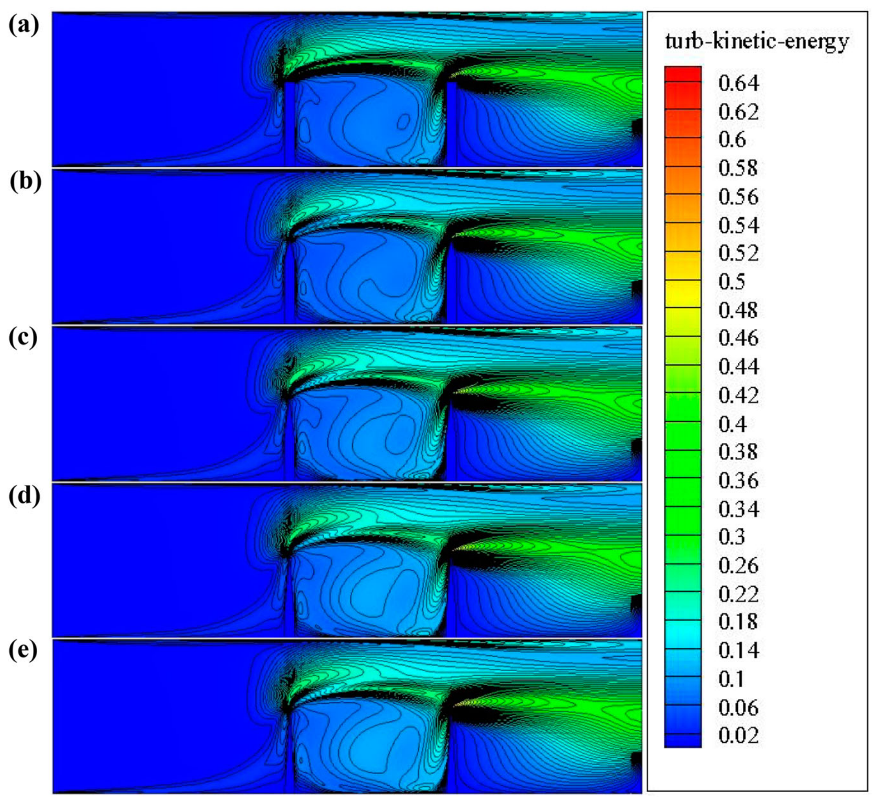

Figure 8. Variation of the turbulent kinetic energy fields at $Re = 12{,}000$, for (a) $a/b = 0.00$, (b) $a/b = 0.25$, (c) $a/b = 0.50$, (d) $a/b = 0.75$, and (e) $a/b = 1.00$.

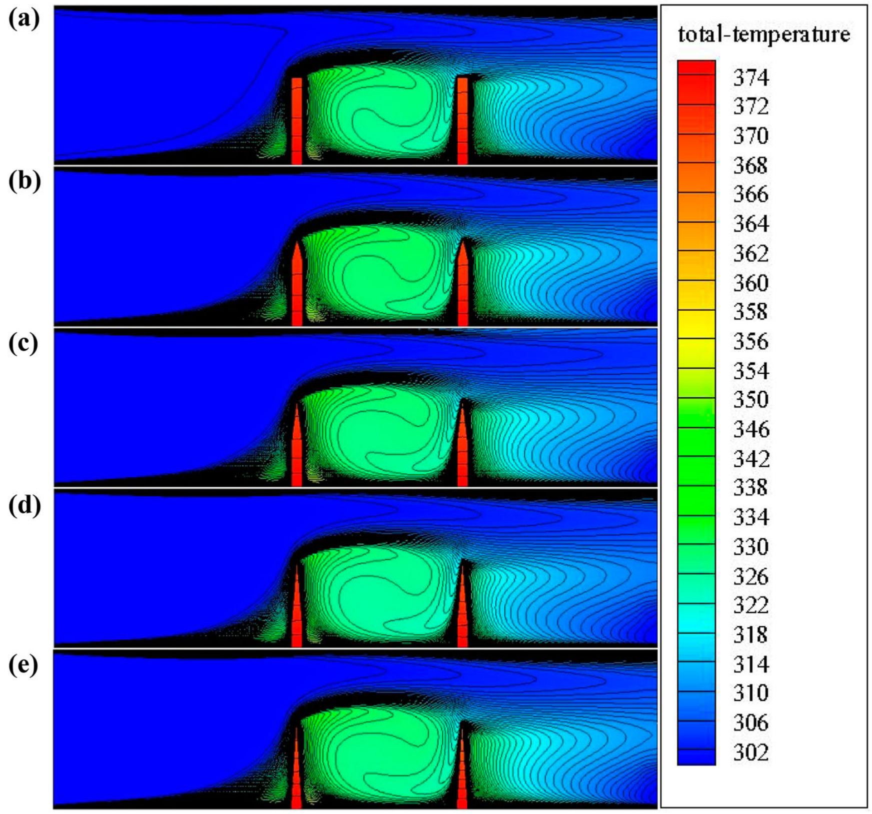

Figure 9. Thermal fields at $Re = 12{,}000$, for (a) $a/b = 0.00$, (b) $a/b = 0.25$, (c) $a/b = 0.50$, (d) $a/b = 0.75$, and (e) $a/b = 1.00$.

Results and discussion

The overall performances of a heat exchanger depend on the working fluid, as well as the geometrical parameters (Abadi et al., 2020; Ramezanizadeh et al., 2019). The turbulent characteristics of a CHE with two in-line deflectors are evaluated in the present paper. Five different cases ($a/b = 0.00$, 0.25, 0.5, 0.75, and 1.00) are considered concerning the shape of deflectors. The results are reported for various Reynolds numbers and for the five mentioned cases in the form of streamlines and contours of velocity, dynamic pressure, turbulent kinetic energy and isotherms. The variations of friction factor, Nusselt number, and hydrothermal enhancement factor are also analyzed.

Hydrothermal fields

The stream function fields for the cases $a/b = 0.00$, 0.25, 0.5, 0.75, and 1.00, at $Re = 1.2 \times 10^4$ are shown in Figure 5a–e, respectively.

As observed, the streamlines are disturbed near the deflectors on their left and right sides for all studied cases. In the region before the first deflector, the airflow is disturbed near its left side. The presence of a deflector on the lower section of the exchanger allows the current to be directed towards the top region while forming a small recirculation loop at the bottom of the deflector. The current moves over the first deflector, splitting at the front of the sharp edge of the same deflector with the formation of an intense recycling cell on its right side. These cells extend to the left wall of the second deflector. In addition, a large recycling cell is generated behind the second deflector in the upper part of the exchanger. In this figure, the formation of vortices within the baffled channel is similar in all cases, but with different intensities.

At $Re = 12{,}000$, the velocity fields of air are plotted in Figure 6 for five different sizes of deflectors, namely: $a/b = 0.00$, 0.25, 0.50, 0.75, and 1.00. In the following areas, the air velocities are low next to the right sides of both deflectors due to the existence of the recirculation loops in these regions. In the area between the deflector tip and the upper surface of the exchanger, an increase in the axial velocity is observed due to the limitation of the flow passage that is resulted by the presence of deflectors.

At the same Re number, the change in the dynamic pressure (P) is plotted in Figure 7 for three types of deflectors (flat, cascaded, and triangular) in an in-line arrangement. As expected, the most significant amount of pressure (P_{max}) is obtained at the upper part of the channel, through the gaps, next to its top wall, due to the

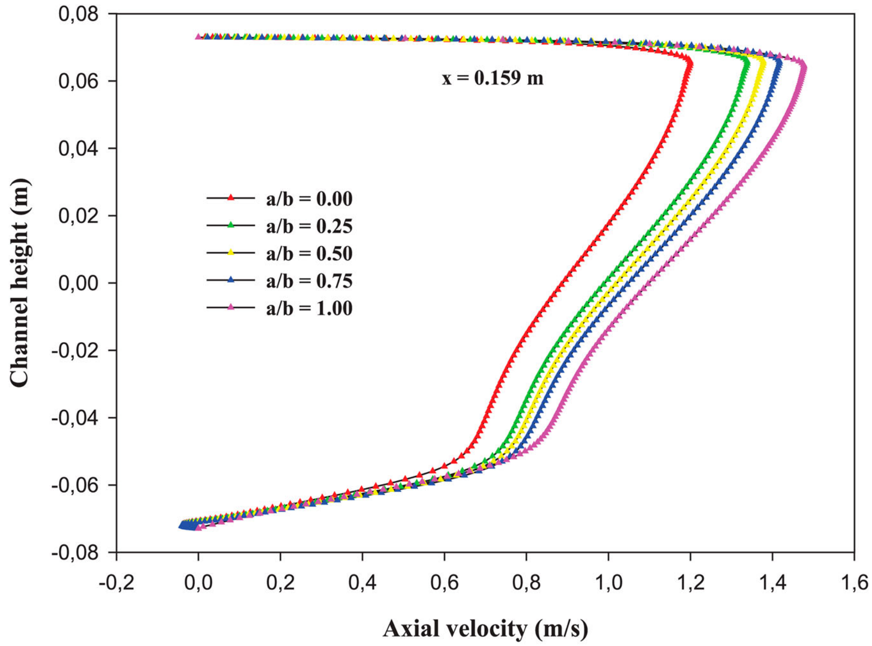

(a)

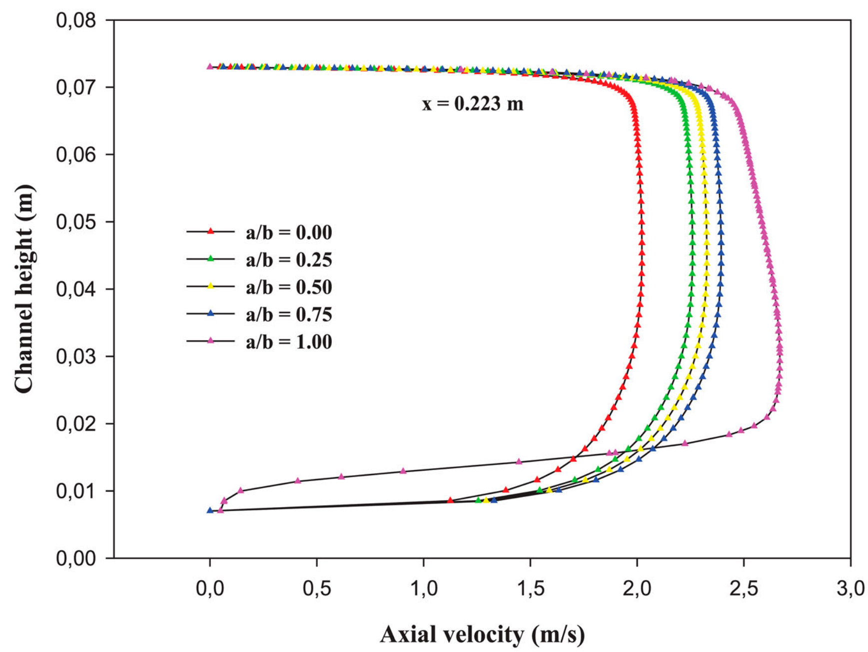

(b)

Figure 10. Axial velocity profiles vs. *a/b* at $Re = 12{,}000$ and (a) $x = 0.159$ m, (b) $x = 0.223$ m, (c) $x = 0.285$ m, (d) $x = 0.315$ m, (e) $x = 0.375$ m, (f) $x = 0.525$ m.

intense velocity in these regions. While the P_{min} value is observed in the recirculation regions that are located in the lower part, next to the right and left walls of both deflectors.

The distribution of turbulence kinetic energy (k) is highlighted in Figure 8 for the five considered values of *a/b*. In this figure, the Reynolds number is fixed at $Re = 12{,}000$. For all cases studied, the k_{max} is found near the front top sharp edges of the first and second deflectors. However, the k_{min} value is located in the upstream and downstream regions of the deflector, for all cases.

The isotherms are shown in Figure 9 for the five different *a/b* ratios. For all cases under investigation, small values of the temperature are remarked in the spaces between the tip of each deflector and the upper wall of

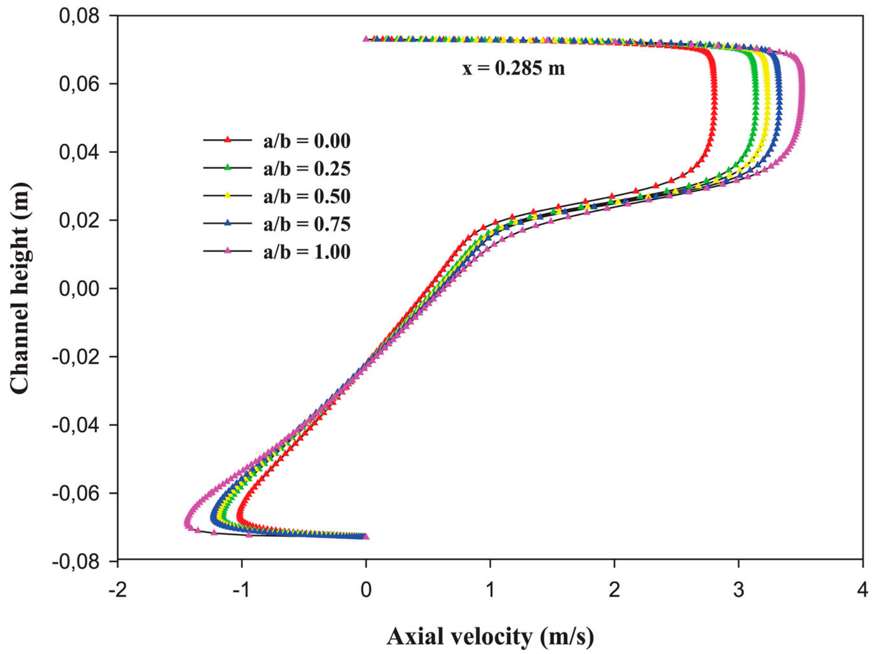

(c)

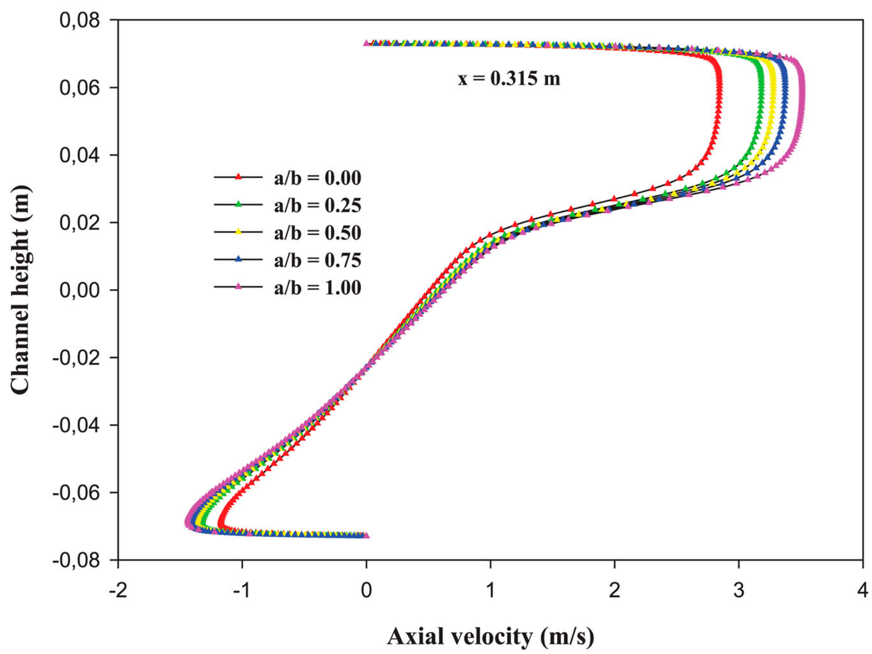

(d)

Figure 10. Continued.

channel. Moreover, the isotherms show that the vortex fluid temperature in the followed regions of the deflector is higher than that obtained in the same region of the smooth channel.

Axial velocity profiles in various stations

Figure 10 highlights the axial velocity (u) profiles of air at the cross sections $x = 0.159$, 0.223, 0.285, 0.315, 0.375, and 0.525 m for $a/b = 0.00$, 0.25, 0.50, 0.75, and 1.00, respectively. At the axial location $x = 0.159$ m, i.e. before the first deflector, the airflow is highly intensified in the top region channel, approaching 114.61–141.12% of the inlet velocity (Figure 10a). However, and in the bottom part of channel, the velocity drops as the flow approaches the first deflector.

Figure 10b addresses the variation of axial velocity(u) in the cross-section starting from the upper wall of the channel to the tip of the first deflector, at $x = 0.223$ m. A strong relationship between the fluid velocity and

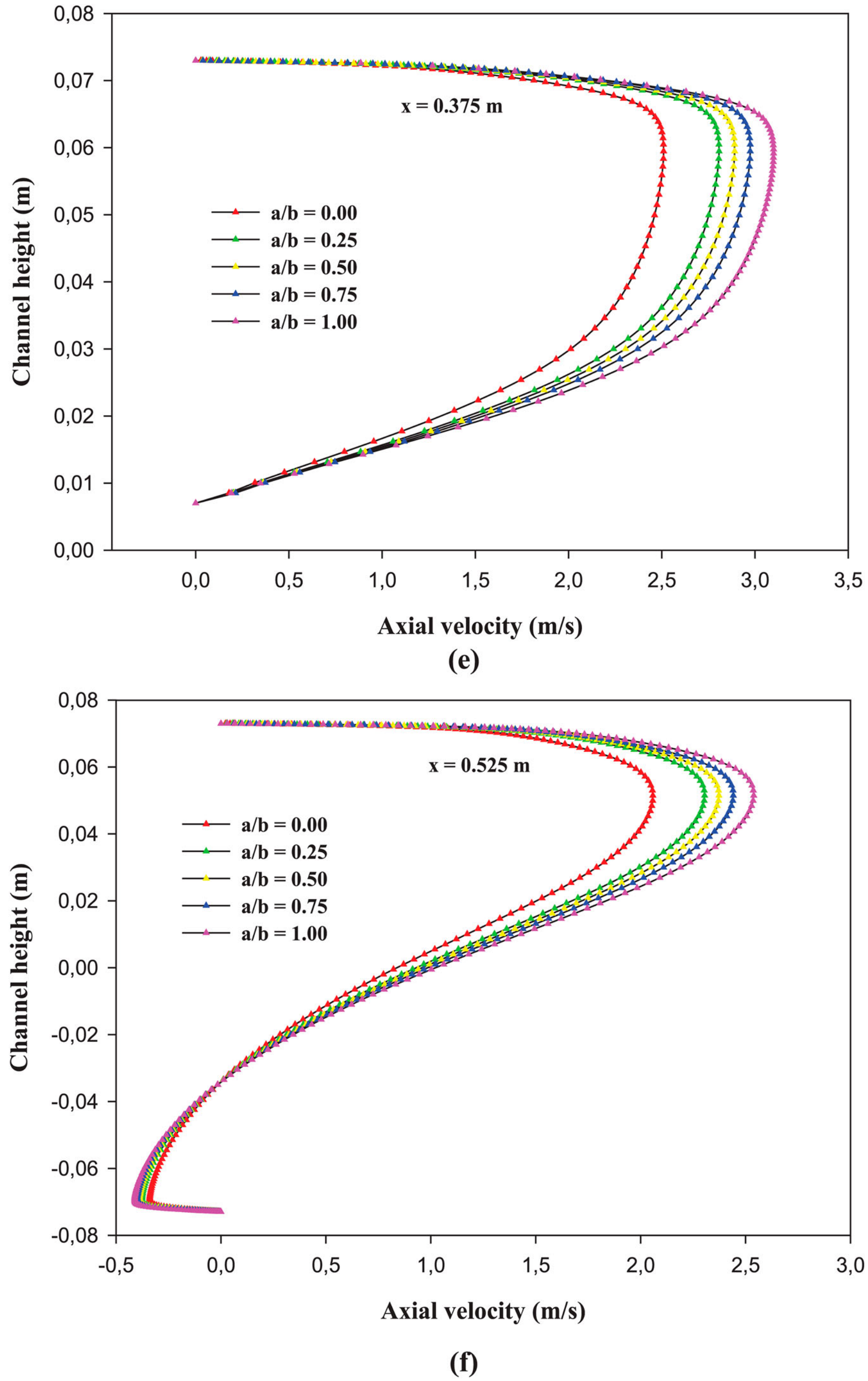

Figure 10. Continued.

the ratio a/b is observed in this figure. In terms of improved velocities, the inclusion of in-line deflectors in its triangular geometry ($a/b = 1.00$) performs better than that of the other deflector cases. The u value in the case $a/b = 1.00$ is found to be higher by about 18.89, 9.39, 6.71, and 4.03% over the air baffled channel with $a/b = 0.00$, 0.25, 0.5, 0.75, and 1.00, respectively. After the first obstacle, at $x = 0.218$, 0.285, and 0.315 m from the channel inlet, there is appearance of recycling cells in the bottom channel area with low negative values of velocity. These vortices are extended with the changes of the obstacle geometry from the flat rectangular form ($a/b = 0.00$) to the triangular from ($a/b = 1.00$). In the upper part of the exchanger, the air current starts to accelerate toward the gap formed between the tip of the second deflector and the opposite wall (Figure 10c and d). In addition, the cascaded rectangular-triangular geometry of the obstacle in the case $a/b = 0.75$ shows most

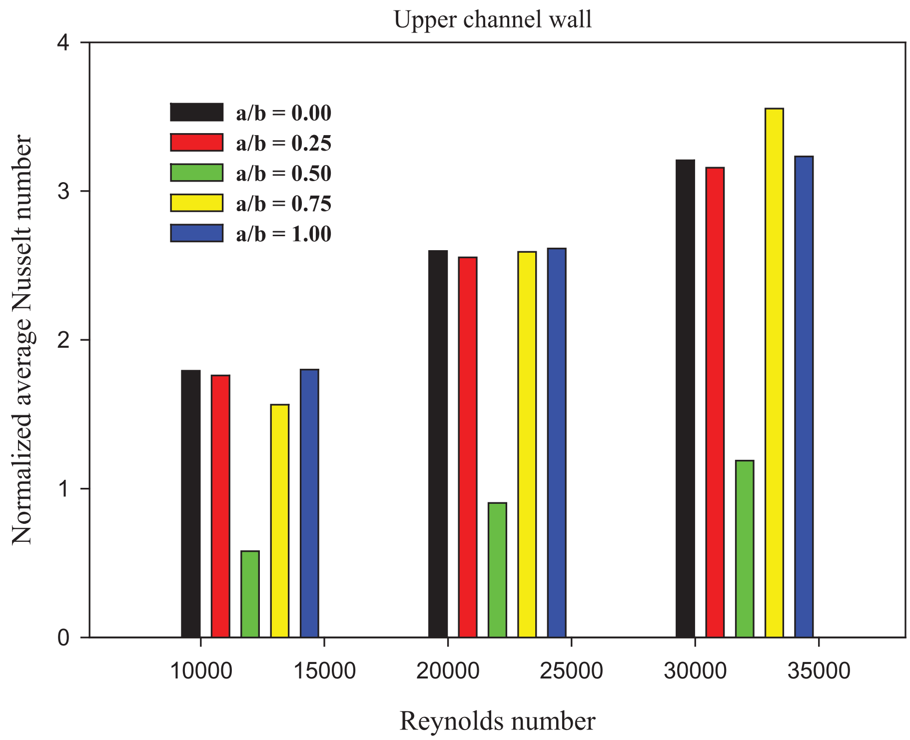

Figure 11. Nusselt number vs. Reynolds number for several deflectors.

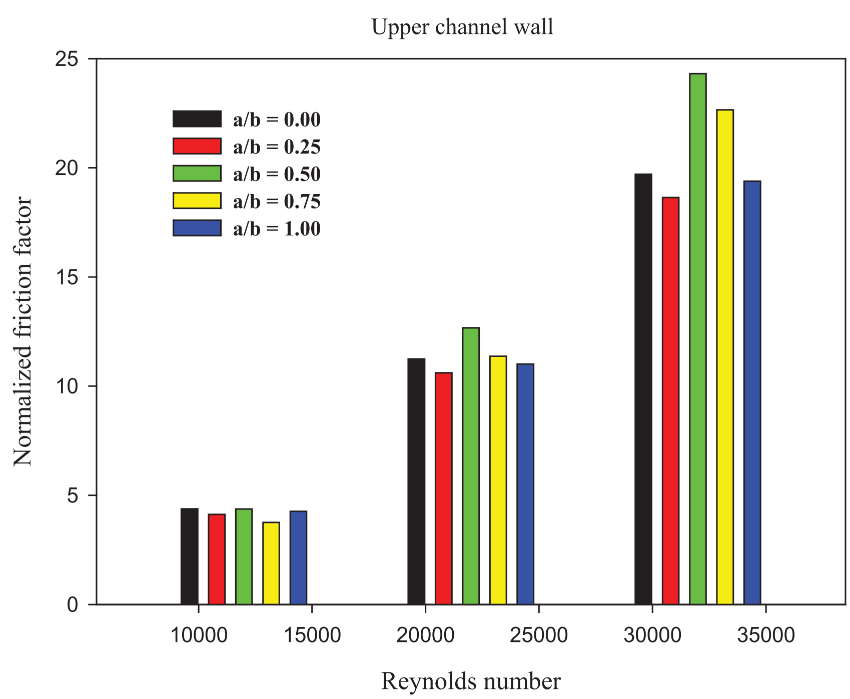

Figure 12. Friction factor vs. Reynolds number for different deflectors.

significant speeds than that in the cases $a/b = 0.25$ and 0.50 by about 106.00 and 102.91%, respectively.

At the axial location $x = 0.375$ m, the profiles of u-velocity in the second space starting from the tip of the second deflector to the upper surface of the exchange rare reported in Figure 10e. The analysis of this figure reveals that the speed increases when changing a/b from 0.00 (or flat rectangular geometry obstacle) to 1.00 (or triangular geometry obstacle). At $x = 0.525$ m, i.e. next to the channel outlet (Figure 10f), the flat rectangular and cascaded rectangular-triangular obstacles ($a/b = 0.25$–0.75) show a decrease in the axial velocity by about 18.78–18.96

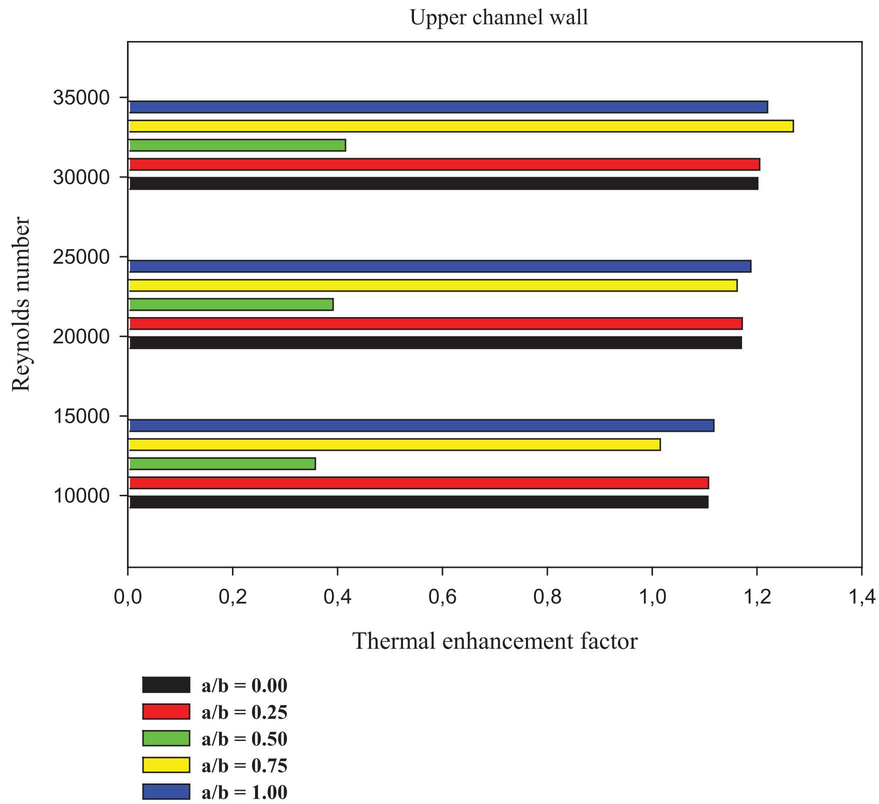

Figure 13. Thermal enhancement performances for different vortex generators.

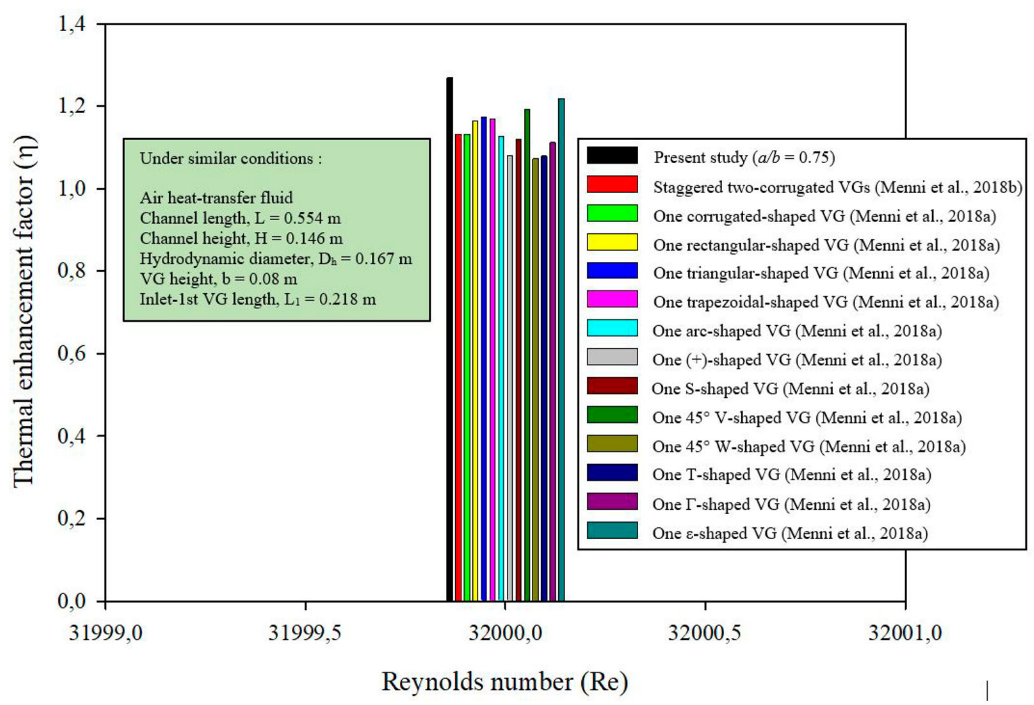

Figure 14. Comparison of the performance of the deflectors' optimal model with the literature given for the highest Reynolds number ($Re = 32{,}000$).

and 3.89–9.37%, respectively, compared to the triangular obstacle ($a/b = 1.00$).

Heat transfer characteristics

Effect of the variation of Reynolds number and obstacle size ($a/b = 0.00$, 0.25, 0.5, 0.75 and 1.00) on Nu is plotted and reported in Figure 11. As expected, the value of Nu/Nu_0 augments with the raise of Re value in all cases studied. The $Nu_{\max}$ is obtained for $a/b = 0.75$ at $Re = 32{,}000$, while the $Nu_{\min}$ is reached at $a/b = 0.50$ for all Re values. At $Re = 32{,}000$, the improvements in Nu values for $a/b = 0.00$, 0.25, 0.5, 0.75 and 1.00, respectively, are about 320.73, 315.73, 118.79, 355.43, and 323.33% over the smooth channel. The inclusion of obstacles with $a/b = 0.75$ at $Re = 32{,}000$ gives high Nu values than that with $a/b = 0.00$, 0.25, 0.50, and 1.00 around 9.76, 11.16, 66.57, and 9.03%, respectively.

Friction loss

The impact of the deflector geometry and Reynolds number on the normalized average skin friction coefficient (f/f_0) is highlighted in Figure 12. An enhancement in f values ranging from 3.75 to 24.31 times over the smooth channel is obtained. The amount of f at $Re = 32{,}000$ and $a/b = 0.50$ is found to be around 18.96, 23.31, 7.31, and 20.26% higher than that with $a/b = 0.00$, 0.25, 0.75, and 1.00, respectively.

Effect of shape on performance

Figure 13 reports the changes in the thermal enhancement factor (η)vs Re for all geometrical configurations under study. H augments with the raise of Re. At $Re = 32{,}000$, the insertion of deflectors with $a/b = 0.75$ yields the most significant η. However, the deflectors with $a/b = 0.50$ yield the lowest η for all Re values considered here. At $Re = 32{,}000$, the most significant values of η is reached with $a/b =$ 0.75, which is higher by about 5.36, 5.06, 67.27, and 3.88%, compared to $a/b = 0.00$, 0.25, 0.50, and 1.00, respectively.

Moreover, the optimum fin case, obtained with $a/b = 0.75$, is compared with various deflector models (Figure 14) from the literature (Menni et al., 2018a, 2018b). Under the same simulated conditions, the 0.75-cascaded model shows an improvement in the performance over all other deflector cases. At $Re = 32{,}000$, the cascaded rectangular-triangular deflector case ($a/b =$ 0.75) shows an increase in the enhancement factor (η) by about 10.795, 8.274, 7.486, 7.880, 11.189, 14.814, 11.662, 6.146, 15.445, 14.972, 12.371, 4.018 and 10.795% compared to the cases of one deflector (corrugated, rectangular, triangular, trapezoidal, arc, (+), S, 45° V, 45° W, T, Γ, and ε-shaped) or two deflectors (staggered corrugated), respectively. This highlights the effectiveness of in-line cascaded rectangular-triangular deflectors with $a/b = 0.75$ in improving the performance of the proposed exchanger for the conditions adopted.

Conclusion

The hydrothermal characteristics of turbulent air flow inside a channel heat exchanger were determined with the CFD computations. The exchanger was equipped with deflectors to enhance the overall performances. Various geometrical configurations concerning the inserted deflectors, as well as various Reynolds numbers were considered in an attempt to augment the thermal enhancement factor. From all calculations, the main findings may be summarized as follows:

- The distribution of streamlines within the channel was similar in all cases through the formation of vortices, but with various intensities.
- The $P_{\max}$ value was observed at the upper part of the channel, through the spaces, next to the top wall due to the intense flow velocity in these regions. However, the $P_{\min}$ value was found in the recirculation loops that are formed in the lower part of channel, next to the right and left walls of both deflectors.
- The $k_{\max}$ was found near the tip of each deflector for all cases studied. However, the $k_{\min}$ value was observed in the upstream, and downstream regions of deflectors for all cases studied.
- The isotherms showed that the air temperature in the area behind the deflectors was higher than that obtained in the same region for the smooth channel.
- At $Re = 32{,}000$, the inclusion of deflectors with $a/b = 0.75$ has given higher Nu values than those with $a/b = 0.00$, 0.25, 0.50, and 1.00 around 9.76, 11.16, 66.57, and 9.03%, respectively.
- The f value at $Re = 32{,}000$ and $a/b = 0.50$ was found to be higher by about 18.96, 23.31, 7.30, and 20.26% than those with $a/b = 0.00$, 0.25, 0.75, and 1.00, respectively.
- The most significant *TEF* was reached at $Re = 32{,}000$ and with $a/b = 0.75$, which was higher by about 5.36, 5.06, 67.27, and 3.88% compared to $a/b = 0.00$, 0.25, 0.50 and, 1.00, respectively.
- At $Re = 32{,}000$, the cascaded rectangular-triangular deflector case ($a/b = 0.75$) showed an increase in the enhancement factor (η) by about 10.795, 8.274, 7.486, 7.880, 11.189,14.814, 11.662, 6.146, 15.445, 14.972,

12.371, 4.018 and 10.795% compared to the cases of one deflector (corrugated, rectangular, triangular, trapezoidal, arc, (+), S, 45° V, 45° W, T, Γ, and ε-shaped) or two deflectors (staggered corrugated), respectively.
- This improvement in the thermal enhancement factor highlights the effectiveness of in-line cascaded rectangular-triangular deflectors with $a/b = 0.75$ in improving the performance of the proposed exchanger for the conditions adopted.

This study may be extended by examining the effect of thermo physical properties of the working fluids, as well as the dimensions, inclination, and arrangement (in-line/staggered) of porous cascaded fins on the overall performances. The combination of fin, nanofluid, and porous media techniques may be also an interesting subject for future works on the enhancement of the performance of channel heat exchangers.

Disclosure statement

The authors declare that they have no conflict of interest.

Nomenclature

b	Deflector height, *m*
C_p	Specific heat capacity, $\mathrm{J\,kg^{-1}\,K^{-1}}$
c_1	Constant of standard k-ε model
c_2	Constant of standard k-ε model
D_h	Hydraulic diameter, *m*
f	Baffled channel friction factor
f_0	Smooth channel friction factor
H	Height of the exchanger, *m*
h_x	Local heat transfer coefficient, $\mathrm{W\,m^2\,K^{-1}}$
k	Turbulent kinetic energy, $\mathrm{m^2\,s^{-2}}$
L	Length of the exchanger, *m*
L_1	Inlet-1stdeflector distance, *m*
L_2	2nd deflector-outlet distance, *m*
Nu	Baffled channel average Nusselt number
Nu_x	Local Nusselt number
Nu_0	Smooth channel Nusselt number
P_{atm}	Atmospheric pressure, *Pa*
Pi	Spacing, *m*
Pr	Prandtl number
Pr_t	Turbulent Prandtl number
Re	Reynolds number
S_ϕ	Source term
t	Deflector thickness, *m*
T	Temperature, *K*
T_{in}	Inlet fluid temperature, *K*
T_w	Wall temperature, *K*
u	Velocity in the axial direction, $\mathrm{m\,s^{-1}}$
U_{in}	Inlet velocity, $\mathrm{m\,s^{-1}}$
v	Velocity in the streamwise direction, $\mathrm{m\,s^{-1}}$
W	Width of the exchanger, *m*

Greek symbols

ϕ	Vector composed of the scalars u, v, T, k, and ε
η	Thermal enhancement factor
ε	Turbulent dissipation rate, $\mathrm{m^2\,s^{-3}}$
ρ_f	Fluid density, $\mathrm{Kg\,m^{-3}}$
Γ_ϕ	Turbulent diffusion coefficient
λ_f	Thermal conductivity, $\mathrm{W\,m^{-1}\,K^{-1}}$
μ_f	Kinematic viscosity, $\mathrm{Kg\,m^{-1}\,s^{-1}}$
μ_e	Effective viscosity, $\mathrm{Kg\,m^{-1}\,s^{-1}}$
μ_l	Laminar viscosity, $\mathrm{Kg\,m^{-1}\,s^{-1}}$
μ_t	Turbulent viscosity, $\mathrm{Kg\,m^{-1}\,s^{-1}}$
ΔP	Pressure drop, *Pa*
σ_k	Constant of standard k-ε model for k
σ_ε	Constant of standard k-ε model for ε
σ_T	Constant of standard k-ε model for T

Subscripts

atm	Atmospheric
e	Effective
f	Fluid
h	Hydraulic
in	Inlet
l	Laminar
t	Turbulent
w	Wall

ORCID

Younes Menni http://orcid.org/0000-0003-1475-3743
Mohammad Hossein Ahmadi http://orcid.org/0000-0002-0097-2534

References

Abadi, A. M. E., Sadi, M., Farzaneh-Gord, M., Ahmadi, M. H., Kumar, R., & Chau, K.-w. (2020). A numerical and experimental study on the energy efficiency of a regenerative Heat and Mass Exchanger utilizing the counter-flow Maisotsenko cycle. *Engineering Applications of Computational Fluid Mechanics*, *14*(1), 1–12. https://doi.org/10.1080/19942060.2019.1617193

Alam, T., & Kim, M. H. (2017). Performance improvement of double-pass solar air heater – A state of art of review. *Renewable and Sustainable Energy Reviews*, *79*, 779–793. https://doi.org/10.1016/j.rser.2017.05.087

Alfellag, M. A., Ahmed, H. E., & Kherbeet, A. S. (2020). Numerical simulation of hydrothermal performance of minichannel heat sink using inclined slotted plate-fins and triangular pins. *Applied Thermal Engineering*, *164*, 114509. https://doi.org/10.1016/j.applthermaleng.2019.114509

Ameur, H. (2019). Effect of the baffle inclination on the flow and thermal fields in channel heat exchangers. *Results in Engineering*, *3*, 100021. https://doi.org/10.1016/j.rineng.2019.100021

Ameur, H. (2020). Effect of corrugated baffles on the flow and thermal fields in a channel heat exchanger. *Journal of Applied and Computational Mechanics*, *6*(2), 209–218. https://doi.org/JACM.2019.28936.1521.

Ameur, H., & Menni, Y. (2019). Laminar cooling of shear thinning fluids in horizontal and baffled tubes: Effect of perforation in baffles. *Thermal Science and Engineering Progress*, *14*, 100430. https://doi.org/10.1016/j.tsep.2019.100430

ANSYS Fluent 12.0. *Theory guide*, Ansys Inc., 2012.

Ary, B. K. P., Lee, M. S., Ahn, S. W., & Lee, D. H. (2012). The effect of the inclined perforated baffle on heat transfer and flow patterns in the channel. *International Communications in Heat and Mass Transfer*, *39*(10), 1578–1583. https://doi.org/10.1016/j.icheatmasstransfer.2012.10.010

Awais, M., & Bhuiyan, A. A. (2018). Heat transfer enhancement using different types of vortex generators (VGs): A review on experimental and numerical activities. *Thermal Science and Engineering Progress*, *5*, 524–545. https://doi.org/10.1016/j.tsep.2018.02.007

Bopche, S. B., & Tandale, M. S. (2009). Experimental investigations on heat transfer and frictional characteristics of a turbulator roughened solar air heater duct. *International Journal of Heat and Mass Transfer*, *52*(11-12), 2834–2848. https://doi.org/10.1016/j.ijheatmasstransfer.2008.09.039

Boukhadia, K., Ameur, H., Sahel, D., & Bozit, M. (2018). Effect of the perforation design on the fluid flow and heat transfer characteristics of a plate fin heat exchanger. *International Journal of Thermal Sciences*, *126*, 172–180. https://doi.org/10.1016/j.ijthermalsci.2017.12.025

Davari, A., & Maerefat, M. (2016). Numerical analysis of fluid flow and heat transfer in entrance and fully developed regions of a channel with porous baffles. *Journal of Heat Transfer*, *138*(6), 062601. https://doi.org/10.1115/1.4032638

Demartini, L. C., Vielmo, H. A., & Möller, S. V. (2004). Numeric and experimental analysis of the turbulent flow through a channel with baffle plates. *Journal of the Brazilian Society of Mechanical Sciences and Engineering*, *26*(2), 153–159. https://doi.org/10.1590/S1678-58782004000200006

Dittus, F. W., & Boelter, L. M. K. (1930). Heat transfer in automobile radiators of the tubular type. *International Communications in Heat and Mass Transfer*, *12*(1), 3–22. https://doi.org/10.1016/0735-1933(85)90003-X

Dutta, P., & Hossain, A. (2005). Internal cooling augmentation in rectangular channel using two inclined baffles. *International Journal of Heat and Fluid Flow*, *26*(2), 223–232. https://doi.org/10.1016/j.ijheatfluidflow.2004.08.001

Eiamsa-Ard, S, & Chuwattanakul, V. (2020). Visualization of heat transfer characteristics using thermochromic liquid crystal temperature measurements in channels with inclined and transverse twisted-baffles. *International Journal of Thermal Sciences*, *153*, 106358.

Gholami, A., Mohammed, H. A., Wahid, M. A., & Khiadani, M. (2019). Parametric design exploration of fin-and-oval tube compact heat exchangers performance with a new type of corrugated fin patterns. *International Journal of Thermal Sciences*, *144*, 173–190. https://doi.org/10.1016/j.ijthermalsci.2019.05.022

Hanna, S. R., Tehranian, S., Carissimo, B., Macdonald, R. W., & Lohner, R. (2002). Comparisons of model simulations with observations of mean flow and turbulence within simple obstacle arrays. *Atmospheric Environment*, *36*(32), 5067–5079. https://doi.org/10.1016/S1352-2310(02)00566-6

Hosseinirad, E., Khoshvaght-Aliabadi, M., & Hormozi, F. (2019). Evaluation of heat transfer and pressure drop in a mini-channel using transverse rectangular vortex-generators with various non-uniform heights. *Applied Thermal Engineering*, *161*, 114196. https://doi.org/10.1016/j.applthermaleng.2019.114196

Huang, X., Chen, L., Kong, Y., Yang, L., & Du, X. (2018). Effects of geometric structures of air deflectors on thermo-flow performances of air-cooled condenser. *International Journal of Heat and Mass Transfer*, *118*, 1022–1039. https://doi.org/10.1016/j.ijheatmasstransfer.2017.11.071

Hwang, R. R., Chow, Y. C., & Peng, Y. F. (1999). Numerical study of turbulent flow over two-dimensional surface-mounted ribs in a channel. *International Journal for Numerical Methods in Fluids*, *31*(4), 767–785. https://doi.org/10.1002/(SICI)1097-0363(19991030)31:4 < 767::AID-FLD902 > 3.0.CO;2-A

Kabeel, A. E., Hamed, M. H., Omara, Z. M., & Kandeal, A. W. (2017). Solar air heaters: Design configurations, improvement methods and applications – A detailed review. *Renewable and Sustainable Energy Reviews*, *70*, 1189–1206. https://doi.org/10.1016/j.rser.2016.12.021

Kadari, A., Chemloul, N. E. S., & Mekroussi, S. (2018). Numerical investigation of Laminar natural convection in a square cavity with wavy wall and horizontal fin attached to the hot wall. *Journal of Heat Transfer*, *140*(7), 072503. https://doi.org/10.1115/1.4039081

Kaewkohkiat, Y., Promvonge, P., & Eiamsa-ard, S. (2017). Turbulent periodic flow and heat transfer in a rectangular channel with detached V-baffles. *Journal of Engineering Thermophysics*, *26*(4), 542–552. https://doi.org/10.1134/S1810232817040099

Karmakar, S., & Mohanty, A. (2019). 2D numerical analysis of natural convection in vertical fins on horizontal base. In D. Srinivasacharya, & K. Reddy (Eds.), *Numerical heat transfer and fluid flow. Lecture notes in mechanical engineering*. Springer. https://doi.org/10.1007/978-981-13-1903-7_48

Khan, J. A., Hinton, J., & Baxter, S. C. (2002). Enhancement of heat transfer with inclined baffles and ribs combined. *Journal of Enhanced Heat Transfer*, *9*(3-4), 137–151. https://doi.org/10.1615/JEnhHeatTransf.v9.i3-4.40

Launder, B. E., & Spalding, D. B. (1974). The numerical computation of turbulent flows. *Computer Methods in Applied Mechanics and Engineering*, *3*(2), 269–289. https://doi.org/10.1016/0045-7825(74)90029-2

Lee, S. J., Lee, S., & Hassan, Y. A. (2018). Numerical investigation of turbulent flow in an annular sector channel with staggered semi-circular ribs using large eddy simulation. *International Journal of Heat and Mass Transfer*, *123*, 705–717. https://doi.org/10.1016/j.ijheatmasstransfer.2018.03.026

Leonard, B. P., & Mokhtari, S. (1990). *ULTRA-SHARP nonoscillatory convection schemes for high-speed steady multidimensional flow*. NASA TM 1-2568, NASA Lewis Research Center.

Li, F., Ma, Q., Xin, G., Zhang, J., & Wang, X. (2020a). Heat transfer and flow characteristics of microchannels with solid and porous ribs. *Applied Thermal Engineering*, *178*, 115639. https://doi.org/10.1016/j.applthermaleng.2020.115639

Liu, J., Hussain, S., Wang, W., Wang, L., Xie, G., & Sunden, B. (2019). Heat transfer enhancement and turbulent flow in a rectangular channel using perforated ribs with inclined holes. *Journal of Heat Transfer*, *141*(4), 041702. https://doi.org/10.1115/1.4042841

Liu, H., & Wang, J. (2011). Numerical investigation on synthetical performances of fluid flow and heat transfer of semiattached rib-channels. *International Journal of Heat and Mass Transfer*, *54*(1-3), 575–583. https://doi.org/10.1016/j.ijheatmasstransfer.2010.09.013

Menni, Y., Ameur, H., Chamkha, A. J., Inc, M., & Almohsen, B. (2020c). Heat and mass transfer of oils in baffled and finned ducts. *Thermal Science*, *24*(Suppl. 1), 267–276. https://doi.org/10.2298/TSCI20S1267M

Menni, Y., Azzi, A., & Chamkha, A. (2018a). Modeling and analysis of solar air channels with attachments of different shapes. *International Journal of Numerical Methods for Heat & Fluid Flow*, *29*(5), 1815–1845. https://doi.org/10.1108/HFF-08-2018-0435

Menni, Y., Azzi, A., & Chamkha, A. J. (2018b). Aerodynamics and heat transfer over solid-deflectors in transverse, staggered, corrugated-upstream and corrugated-downstream patterns. *Periodica Polytechnica Mechanical Engineering*, *62*(3), 209–217. https://doi.org/10.3311/PPme.11972

Menni, Y., Chamkha, A. J., Ghazvini, M., Ahmadi, M. H., Ameur, H., Issakhov, A., & Inc, M. (2021). Enhancement of the turbulent convective heat transfer in channels through the baffling technique and oil/multiwalled carbon nanotube nanofluids. *Numerical Heat Transfer, Part A: Applications*, *79*(4), 311–351. https://doi.org/10.1080/10407782.2020.1842846

Menni, Y., Ghazvini, M., Ameur, H., Ahmadi, M. H., & Sadeghzadeh, M. S. M. (2020a). Numerical calculations of the thermal-aerodynamic characteristics in a solar duct with multiple V-baffles. *Engineering Applications of Computational Fluid Mechanics*, *14*(1), 1173–1197. https://doi.org/10.1080/19942060.2020.1815586

Menni, Y., Ghazvini, M., Ameur, H., Kim, M., Ahmadi, M. H., & Sharifpur, M. (2020b). Combination of baffling technique and high-thermal conductivity fluids to enhance the overall performances of solar channels. *Engineering with Computers*. https://doi.org/10.1007/s00366-020-01165-x

Mesgarpour, M., Heydari, A., & Saddodin, S. (2018). Investigating the effect of connection type of a sintered porous fin through a channel on heat transfer and fluid flow. *Journal of Thermal Analysis and Calorimetry*, *135*(1), 461–474. https://doi.org/10.1007/s10973-018-7356-y

Misra, R., Singh, J., Jain, S. K., Faujdar, S., Agrawa, M., Mishra, A., & Goyal, P. K. (2020). Prediction of behavior of triangular solar air heater duct using V-down rib with multiple gaps and turbulence promoters as artificial roughness: A CFD analysis. *International Journal of Heat and Mass Transfer*, *162*, 120376. https://doi.org/10.1016/j.ijheatmasstransfer.2020.120376

Nasiruddin, S., & Siddiqui, M. H. K. (2007). Heat transfer augmentation in a heat exchanger tube using a baffle. *International Journal of Heat and Fluid Flow*, *28*(2), 318–328. https://doi.org/10.1016/j.ijheatfluidflow.2006.03.020

Patankar, S. V. (1980). *Numerical heat transfer and fluid flow*. McGraw-Hill.

Petukhov, B. S. (1970). Heat transfer and friction in turbulent pipe flow with variable physical properties. *Advances in Heat Transfer*, *6*, 503–564. https://doi.org/10.1016/S0065-2717(08)70153-9

Phila, A., Eiamsa-ard, S., & Thianpong, C. (2020). Thermal performance evaluation of a channel installed with inclined-baffle turbulators. *Arabian Journal for Science and Engineering*, *45*(2), 609–621. https://doi.org/10.1007/s13369-019-04097-x

Promvonge, P., & Skullong, S. (2020). Thermo-hydraulic performance in heat exchanger tube with V-shaped winglet vortex generator. *Applied Thermal Engineering*, *164*, 114424. https://doi.org/10.1016/j.applthermaleng.2019.114424

Promvonge, P., Tamna, S., Pimsarn, M., & Thianpong, C. (2015). Thermal characterization in a circular tube fitted with inclined horseshoe baffles. *Applied Thermal Engineering*, *75*, 1147–1155. https://doi.org/10.1016/j.applthermaleng.2014.10.045

Promvonge, P., & Thianpong, C. (2008). Thermal performance assessment of turbulent channel flows over different shaped ribs. *International Communications in Heat and Mass Transfer*, *35*(10), 1327–1334. https://doi.org/10.1016/j.icheatmasstransfer.2008.07.016

Ramezanizadeh, M., Alhuyi Nazari, M., Ahmadi, M. H., & Chau, K. W. (2019). Experimental and numerical analysis of a nanofluidic thermosyphon heat exchanger. *Engineering Applications of Computational Fluid Mechanics*, *13*(1), 40–47. https://doi.org/10.1080/19942060.2018.1518272

Wang, Y., Liu, P., Shan, F., Liu, Z., & Liu, W. (2019). Effect of longitudinal vortex generator on the heat transfer enhancement of a circular tube. *Applied Thermal Engineering*, *148*, 1018–1028. https://doi.org/10.1016/j.applthermaleng.2018.11.080

Wang, F., Zhang, J., & Wang, S. (2012). Investigation on flow and heat transfer characteristics in rectangular channel with drop-shaped pin fins. *Propulsion and Power Research*, *1*(1), 64–70. https://doi.org/10.1016/j.jppr.2012.10.003

Yang, Y. T., & Hwang, C. Z. (2003). Calculation of turbulent flow and heat transfer in a porous-baffled channel. *International Journal of Heat and Mass Transfer*, *46*(5), 771–780. https://doi.org/10.1016/S0017-9310(02)00360-5

Yongsiri, K., Eiamsa-ard, P., Wongcharee, K., & Eiamsa-ard, S. (2014). Augmented heat transfer in a turbulent channel flow with inclined detached-ribs. *Case Studies in Thermal Engineering*, *3*, 1–10. https://doi.org/10.1016/j.csite.2013.12.003

Zhao, H., Liu, Z., Zhang, C., Guan, N., & Zhao, H. (2016). Pressure drop and friction factor of a rectangular channel with staggered mini pin fins of different shapes. *Experimental Thermal and Fluid Science*, *71*, 57–69. https://doi.org/10.1016/j.expthermflusci.2015.10.010